Graphical abstract

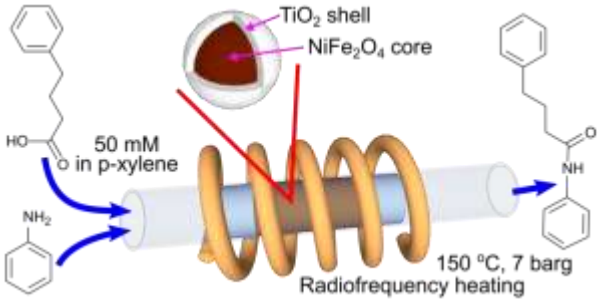

Highlight:

A core-shell TiO_2@$NiFe_2O_4$ catalyst showed high activity and stability in direct amide synthesis with easy regeneration from coke by a treatment with a 30 wt. % hydrogen peroxide solution.

Direct amide synthesis over core-shell TiO_2@$NiFe_2O_4$ catalysts in a continuous flow radiofrequency-heated reactor

Yawen Liu[1], Pengzhao Gao[2], Nikolay Cherkasov[1], Evgeny V. Rebrov [1,3,] *

[1] School of Engineering, University of Warwick, Coventry CV4 7AL, UK

[2] College of Materials Science and Engineering, Hunan University, Changsha 410082, China

[3] Department of Biotechnology and Chemistry, Tver State Technical University, 170026, Nab. A.Nikitina 22, Russia

* E-mail: E.Rebrov@warwick.ac.uk

Abstract

Core-shell composite magnetic catalysts TiO_2@$NiFe_2O_4$ with a titania loading of 9–32 wt. % have been synthesised by sol-gel method for direct amide synthesis in a radiofrequency (RF)-heated continuous flow reactor. The catalyst calcination temperature was optimised in the range of 350-500 ºC and the highest activity was observed for the catalyst calcined at 500 ºC due to conversion of titania into catalytically active anatase phase. No reaction between the magnetic core and the titania shell was observed up to the calcination temperature of 1000 ºC and no sintering of titania shell was observed after calcination at 500 ºC. The comparison of direct amide synthesis in a continuous flow fixed bed reactor under conventional and RF heating demonstrated that the RF heating mode increased the apparent reaction rate by 60 % and decreased the deactivation rate due to a better temperature uniformity. The titania weight normalised reaction rate in the RF-heated reactor was constant for titania loadings above 17 wt. %, while it decreased by a factor of 3 at lower titania loadings because of interactions between the ferrite core on the thin layer of the catalyst. The catalyst deactivation study showed that the deactivation rate could be accurately described by a first order kinetics and that the main reason of deactivation was coking. The catalyst regeneration via calcination at 400 ºC resulted in the catalyst sintering, while a treatment with a hydrogen peroxide solution at 90 ºC fully recovered catalytic activity.

Keywords: sol-gel synthesis; core shell; titania; direct amide synthesis; radiofrequency heating.

1. Introduction

Synthesis of amide molecules is essential in pharmaceutical, medical, biological as well as polymer industries [1-3]. In pharmaceutical industry in particular, the synthesis of 65 % of drug candidates involves the amide bond formation [4]. However, traditional amide synthesis routes require either the synthesis of halogen derivatives or application of coupling agents in order to facilitate the reaction under relatively mild conditions [3, 5, 6]. The main drawback of this approach is the utilization of large, often stoichiometric, amounts of expensive, toxic, halogenated agents which require additional separation stages, resulting in poor atom economy and generation of large amounts of toxic waste. This problem was recognized as the one of most topical problems of pharmaceutical synthesis [4].

A desired scenario for the amide synthesis, the direct reaction between readily available carboxylic acids and amines, is currently very limited because (i) thermal (non-catalytic) synthesis of amides in this way is only possible for a very limited range of reactants, (ii) it requires long reaction time and (iii) high temperature which is usually unacceptable for thermo liable pharmaceutical molecules [7-9]. For example, the amide yield in the reaction between aniline and 4-phenylbutyric acid after 48 hrs is as low as 4 % at 120 ºC [8]. To increase the reaction rate, many metal oxides demonstrated catalytic activity such as CeO_2, CaO, MgO, ZnO, Y_2O_3, TiO_2, ZrO_2, Nb_2O_5, Al_2O_3, SiO_2 [10-13] as well as solid acids like Amberlyst-15, HBEA, niobic acid, mont-K10, nafion-SiO_2 and IBA [10, 14]. Among them, titania provides a unique combination of low price and high catalytic activity [15-17]. Hosseini-Sarvari et al. [15] applied nanosized sulfated titania to direct amide synthesis in a batch reactor using a wide range of substrates and obtained the yields of 70 – 98 % in 3 - 12 h at 115 ºC. Nagarajan et al. [16] demonstrated quick (under 30 min) amide synthesis with the yields ranging from 83 to 98 % using sulfated titania nanotubes at 110 ºC. Microwave heating applied by Gaudino et al. [18] resulted in the product yields over 55 % at 100 ºC within 60 min over a commercial P25 TiO_2 catalyst.

The literature data shows that the application of titania catalysts in direct amide synthesis allows for high amide yields within the reaction time of less than an hour at moderately high reaction temperatures. However, the efficiency of widely studied batch processes is limited for such reaction conditions. In particular, low heat transfer rates via reactor walls in stirred tank reactors may result in non-uniform temperature profile in large reactors with a possibility of hot spot formation in stagnant zones resulting in accelerated catalyst deactivation. Moreover, an inefficient mechanism of heat transfer, conduction through the reactor walls and convection through the reaction solution, results in high energy consumption and increases product costs. A promising solution to these problems lies

with the combination of (i) continuous flow processing coupled with (ii) radiofrequency (RF)-heated reactors.

Small volume of continuous flow reactors provide a substantial increase in heat and mass transfer rates increasing utilization efficiency of the equipment [19, 20]. In addition, flow reactors are intrinsically safe because a rupture of the reactor wall operating even under high pressure results in the release of minute amounts of hazardous substances. This allows for safe handling dangerous materials or a drastic expansion of possible reaction conditions [21]. These advantages result in process intensification, an increase in reaction rates per reactor volume by a factor of 2 to 1000 compared to conventionally used batch systems [21]. As a result, flow reactors with a millilitre-range diameter could produce kilogram quantities of product when operated for a whole day [22]. Flow reactors easily allow to reach and exploit intrinsic limitations on product selectivity of the catalysts, resulting in an increased economic efficiency of the processes [19, 23, 24].

Despite of these advantages, there are very few works which studied amide synthesis in continuous flow. Mascia et al. [25] demonstrated a more than 6-fold decrease in the reaction time (from 300 to 47 h) in a flow compared to a batch reactor using in a homogeneously acid-catalysed reaction of an anhydride with an amine. Furthermore, the overall reaction apparatus was simplified in flow reducing the number of unit operations from 21 to 14 mainly due to simplification in the downstream steps such as pharmaceutical formulation, mixing and granulation. Gustafsson et al. [26] showed feasibility of flow synthesis for a wide range of amides using highly reactive trimethylaluminium agent. Liu and Jensen [27] combined heterogeneous oxidation, gas-liquid separation and oxidation amination for the synthesis of amides from amines and alcohols. However, the complexity of the system required may be a limitation of the approach. Comerford et al. [13] showed the feasibility of the direct amide synthesis from 4-phenylbutyric acid and aniline in continuous flow over an acidic silica catalyst.

The problem of low energy efficiency, which is vital for the processes operating in the temperature above 100 ºC on a large scale, can be significantly improved using non-conventional heating sources like microwave or RF heating [28]. Moreover, when heat is transferred from the walls, the temperature gradient through the cross section may lead to lower temperature in the central part, resulting in low reaction rates. Recently, the RF-heated continuous flow reactor where heat is generated by the magnetic particles in the alternating magnetic field has been applied in the organic synthesis [29-32]. As heat is uniformly generated over the entire catalyst volume, it provides much a smaller radial temperature gradient and reduced heat loss to the environment. Additionally, Ceylan et al. [29] has demonstrated higher yields (80 vs 65 %) of organic reactions conducted in an RF-heated reactor compared to that in a conventional continuous flow reactor. RF heating also provides a

further advantage of catalyst separation simply using a magnet, decreasing the recycle costs of heterogeneous catalysts [33-35].

In our previous contribution, we reported feasibility of the direct amide synthesis conducted in an RF-heated continuous reactor packed with a P25 titania/nickel ferrite catalyst obtained by solid state synthesis [32]. The amide yield of 35 % was demonstrated with optimisation of ball milling time performed. However, the approach of a mixed composite (catalytic and magnetic) particles has its intrinsic limitations. Firstly, magnetic nanoparticles exposed to the reaction medium can be corroded in solutions with high acidity or alkalinity, which decreases the catalyst lifetime and may result in by-product formation. Secondly, the ball milling step used for catalyst preparation provides high mechanical impact on titania nanoparticles resulting in poor control of the catalyst morphology and low surface area. Both problems can be solved with the application of a core-shell catalyst which avoids these problems and has been proved to be efficient in a range of chemistries [36-38]. The aim of this work was to obtain a TiO_2@$NiFe_2O_4$ magnetic composite catalyst with a core-shell structure for direct amide synthesis in an RF-heated continuous reactor, and to optimise its heating and catalytic properties.

2. Experimental

2.1 Synthesis of composite catalysts

The nickel ferrite nanoparticles were synthesized by a sol-gel method [39]. A solution of 51.69 g iron (III) nitrate nonahydrate, 18.6 g nickel (II) nitrate hexahydrate in 250 mL ethanol was mixed with a solution of 36.9 g citric acid in 150 mL ethanol. After stirring the mixture for 24 h, a 2 M ammonia solution was added dropwise to adjust the pH to 2. Under stirring, the temperature was increased to 90 ºC to evaporate the solvent until the total volume decreased to about 150 mL. The slurry was dried further in an oven at 90 ºC, grinded and then calcined in air at 700 ºC for 1 h with a heating rate of 2 ºC min^{-1}. The obtained material (3 g) was dispersed under ultrasound in 300 mL water/ethanol (20:80 v/v) solution of 1 M ammonia and 3 mM cetyltrimethylammonium bromide (CTAB).

The titania sol was prepared mixing 85 mL tetrabutyl titanate, 25 mL diethanolamine and 285 mL ethanol followed by hydrolysis under vigorous stirring caused by dropwise (20 mL h^{-1}) addition of a water/ethanol solution (10 mL/100 mL). The resulting translucent sol was left aging for 24 h under stirring at room temperature and then without stirring for another 24 h.

The core-shell composite catalysts were prepared by adding dropwise (20 mL h^{-1}) the titania sol obtained into the suspension of $NiFe_2O_4$ nanoparticles under vigorous stirring. The solid material

obtained was centrifuged, washed with ethanol (3x20 mL), dried in air at 70 ºC overnight and calcined in air at the desired temperature for 1 h with a heating rate of 1 ºC min^{-1}. The samples obtained are referred to as T-X-Y where index X is the measured titania loading (wt. %) and Y is the calcination temperature in ºC. The first indexes are different for the catalysts recovered after the reaction: spent catalyst (ST); regenerated with a 30 wt. % aqueous solution of H_2O_2, chemically-treated (CT); and thermally regenerated catalysts, thermally-treated (TT).

2.2 Catalyst characterization

Powder X-ray diffraction (XRD) study was performed using a PANalytical Empyrean diffractometer with a Fe-filtered Co Kα radiation (0.179 nm) with a scanning rate of 2^o 2θ min^{-1}. The resulting data were re-calculated into Cu wavelength (0.154 nm) for proper comparison with literature data. The infrared spectra were recorded in transmission mode in the 2000-400 cm^{-1} range and a resolution of 2 cm^{-1} using an Avatar360 Nicolet IR spectrometer. The catalysts (3-5 mg) were mixed with KBr (3-5 mg), pressed into self-supporting wafers and placed in an in-situ cell with CaF_2 windows.

The TiO_2 content in the composite catalysts was determined via an energy dispersive spectrometry (EDS) using a Jeol JSM-6700F scanning electron microscope (Table 1). The powdered materials were applied on an adhesive conductive tape and studied without additional metal coating. The catalyst morphology was studied with a Philips, Tecnan F20 transmission electron microscope operated at 200 kV. The catalysts were dispersed in ethanol under sonication and a droplet of the suspension was applied on the carbon-coated copper grids.

The as-synthesized samples (20 mg) were characterized by combined thermogravimetric and differential thermal analysis (TG-DTA) on a STA 449 C Netzsch Analyser in a 10 mL min^{-1} flow of 20 vol. % O_2/N_2 and a heating rate of 10 ºC min^{-1}. The temperature programmed oxidation analysis was performed for the spent samples placing 50 mg of the sample into a U-shaped quartz tube between plugs of quartz wool. After waiting for 1 h at 25 ºC in the flow of N_2, the flow was switched to a mixture containing 1 vol. % O_2, 1 vol.% Ar (internal standard), and 98 vol. % N_2 and the temperature was increased linearly at a rate of 10 ºC min^{-1}. The concentrations of CO, CO_2 and H_2O were recorded by a quadrupole mass spectrometer.

The magnetic properties of the catalyst were measured at room temperature using a vibrating sample magnetometer, Princeton Measurements Corporation MicroMag 3900 VSM, equipped with a 2 T electromagnet. The saturation magnetization (Ms) was evaluated from the hysteresis loop. The specific absorbtion rate (SAR) under the RF field was determined as the initial thermal power of the

catalyst under RF heating. An insulated glass tube was loaded with 10 mg sample and 50 μL water, placed in the middle of a 5-turn coil and heated with a RF generator (Easyheat 0112, current 200 A). A fibre optics temperature sensor inserted into the sample recorded the temperature increase and the first 30 s of linear temperature increase was used for (SAR) calculation [39].

Table 1. Titania in the catalysts studied: nominal ($\omega_{nominal}$) and determined by EDS (ω_{EDS}).

Sample	$\omega_{nominal}$ (wt. %)	ω_{EDS} (wt. %)
T-9-400	7.4	8.9
T-17-400	13.9	16.7
T-26-400	24.3	26.0
T-32-400	32.5	32.0

2.3 Catalytic activity testing

The catalytic activity of the composite catalysts was measured in the amide synthesis in a 160 mL Parr continuously stirred tank reactor. The catalyst, 680 mg, and the reactants, 50 mM aniline, 50 mM 4-phenylbutyric acid (PBA), 50 mM tetradecane (internal standard) in 100 mL p-xylene, were added into the reactor. The reactor was purged with N_2 on stirring, pressurised to 6 bar with N_2 and heated to 150 ºC. The reaction was carried out at a stirring rate of about 950 min^{-1}. The samples (1-2 mL) were collected at regular intervals. A series of experiments with various stirring rates and catalyst weights confirmed the absence of mass transfer limitations.

The optimized TiO_2@$NiFe_2O_4$ catalysts were tested in a continuous flow reactor. The catalyst, 320 mg, pressed and sieved to obtain the fraction of 125–250 μm, was placed in the central part of the reactor forming a catalyst bed with a length of 5 mm. To preheat the reactant solution, a 5 mm preheating section consisting of catalytically inert iron oxide pellets (pellet size: 125–250 μm) was placed before the catalyst bed. A Fiso FOT-L-SD optic fibre temperature sensor was attached to the outer surface of the reactor, which was insulated with a 1 cm thick layer of glass wool and placed into an 8-turn induction coil connected to an RF generator operating at 223 kHz (Easyheat) The electric current of the RF generator was controlled with a PID controller to provide a constant bed temperature.

The reaction under conventional heating was performed using a resistive heating wire as a heating source. To account for slow conductive heat transfer, the length of the initial pre-heating zone was increased to insure that the inlet feed reaches the catalyst bed at the desired reaction temperature. The p-xylene solutions of aniline (100 mM) and 4-phenylbutyric acid (100 mM along

with 100 mM of tetradecane) were introduced into the reactor at a desired flow rate using two Shimadzu LC-20AD HPLC pumps. The outlet pressure was maintained at 7 bar (gauge) with a back pressure controller to allow operation at temperatures above the normal boiling point of p-xylene. The samples collected were analysed using a gas chromatograph (Shimadzu GC-2010) equipped a 30 m Stabilwax capillary column and a flame ionization detector.

No products other than N, 4-diphenylbutynamide were observed and the carbon balance was better than 98 % according to the scheme presented in Fig 1. The reaction yield was found to be limited (to 60 %) by the product solubility. Hence, all reactions were performed in the conversion range of 10-50 % and the discussion was further focused on the reaction rates.

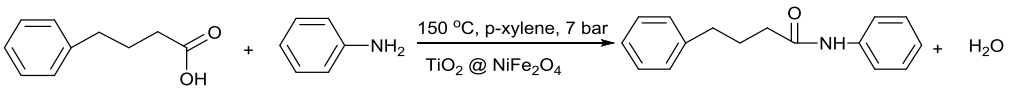

Fig 1. Reaction scheme of the N,4-diphenylbutyramide synthesis.

3. Results and discussion

3.1 Thermal behaviour

Fig 2 shows TG-DTA curves of $NiFe_2O_4$ nanoparticles, dry TiO_2 gel, and composite catalysts. In the studied temperature range, $NiFe_2O_4$ showed no change in weight and low thermal effect demonstrating that the stable phase was obtained by calcination at 700 ºC, which is in agreement with the previous reports [40, 41] (Fig 2a). For the TiO_2 dry gel (Fig 2b), adsorbed ethanol and water were removed in the temperature range of 75 to 165 ºC. The decomposition of the precursors was observed in the range from 270 to 323 ºC followed by oxidation of residual organic materials above 475 ºC [42]. The weight of TiO_2 gel was constant above 570 ºC indicating full removal of combustible materials. The composite catalysts demonstrated behaviour similar to that of the TiO_2 dry gel (Fig 2c) – a continuous weight loss in the temperature range below 570 ºC was observed caused by the removal of solvents and organic precursors. The total weight loss increased from 10.2 to 25.1 % proportionally to TiO_2 content showing that organic materials were primarily adsorbed in the titania layer. The thermal effect above 570 ºC in the composite materials was lower than that of $NiFe_2O_4$ showing the absence of solid-state reactions between the TiO_2 framework and $NiFe_2O_4$ nanoparticles in the composite catalysts.

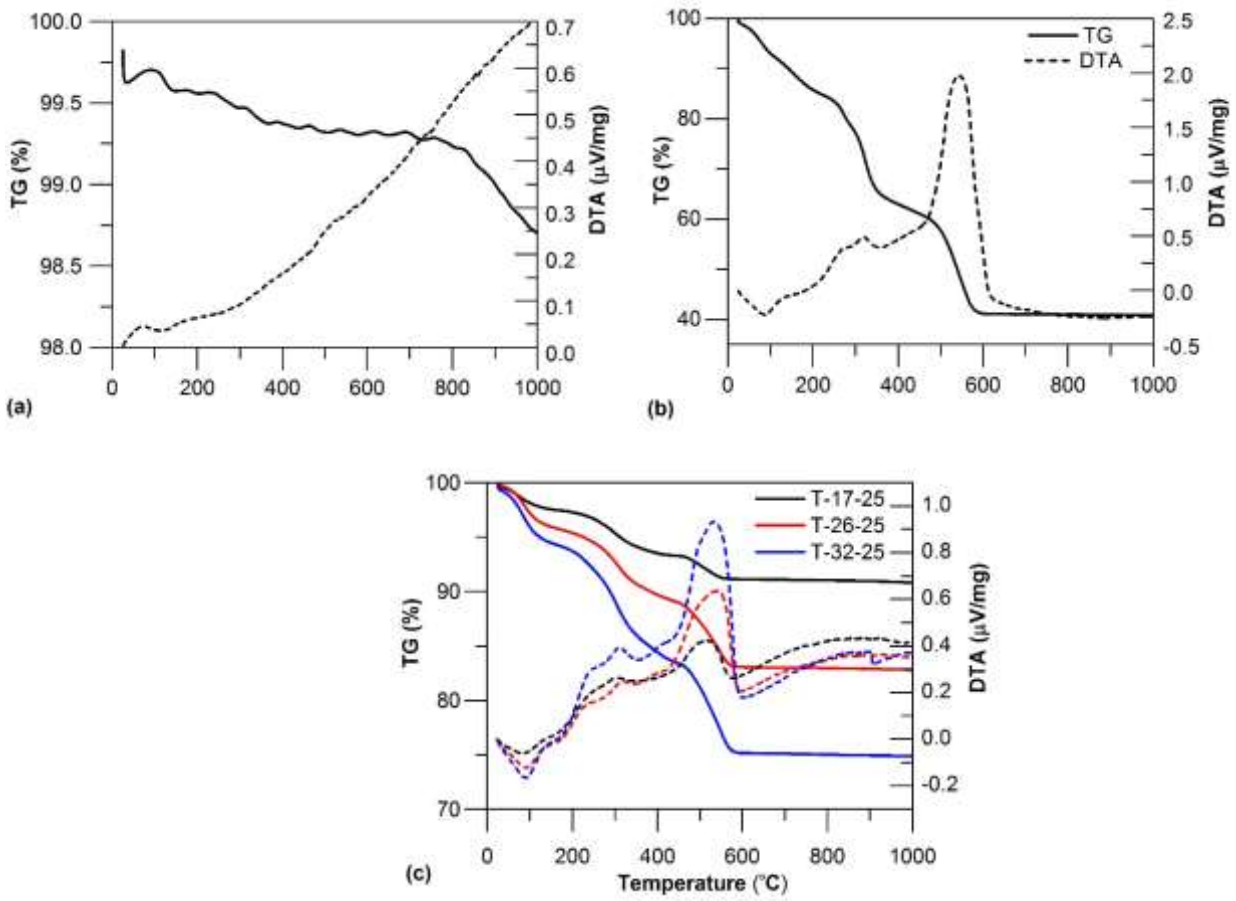

Fig 2. Thermogravimetric analysis (solid curves) and differential thermal analysis (dashed curves) of (a) $NiFe_2O_4$ (b) TiO_2 dry gel (c) as-synthesised composite catalysts T-17-25, T-26-25 and T-32-25 with titania loadings of 16.7, 26 and 32 wt. %, respectively.

3.2 Effect of TiO_2 loading

Four composite catalysts with the TiO_2 loading of 8.9, 16.7, 26.0 and 32.0 wt. % have been prepared to investigate the effect of titania content on their activity and stability in the amide synthesis reaction. The actual TiO_2 content was in good agreement with the nominal composition (Table 1), demonstrating efficient incorporation of TiO_2 sol onto the magnetic nanoparticles. Nearly spherical particles were observed in TEM images of all samples (Fig 3). The titania formed a layer around nickel ferrite nanoparticles (shown with arrows in Figs 3 b-d) with the thickness of about 5-10 nm. The incorporation of titania coating did not change the average dimensions of the $NiFe_2O_4$ core (40–60 nm in diameter), which agrees with the TGA data on the absence of chemical interaction between the core and the shell during the synthesis (Fig 2).

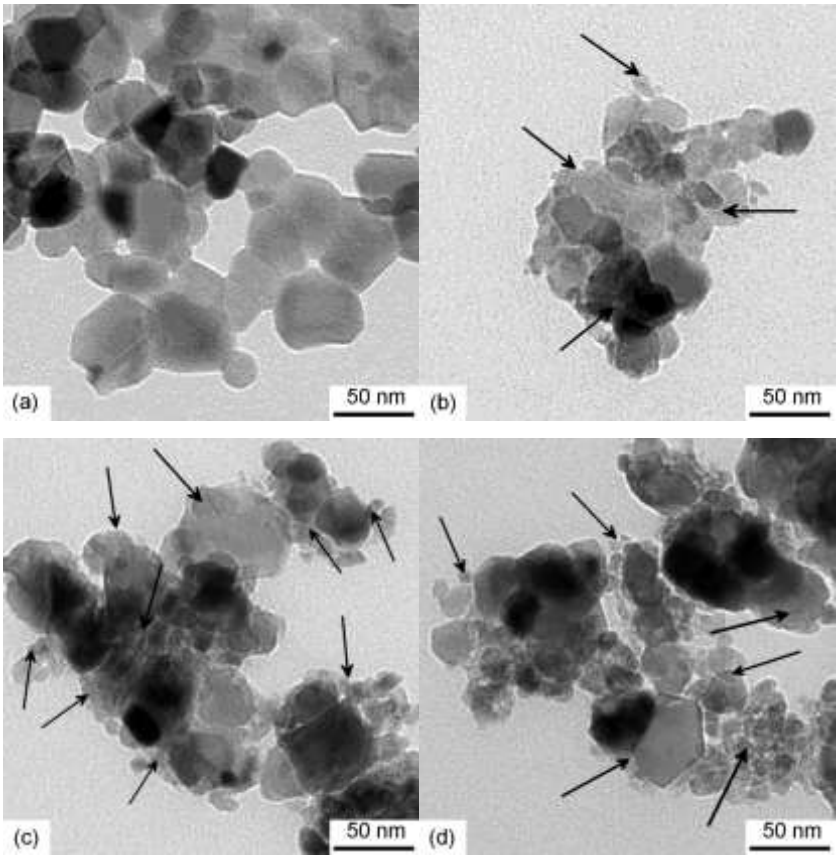

Fig 3. TEM photographs of (a) initial nickel ferrite nanoparticles and (b-d) composite catalysts calcined at 400 ºC with TiO_2 loading of (b) 16.7 wt. %, sample T-17-400, (c) 26 wt. %, sample T-26-400, and (d) 32 wt. %, sample T-32-400. Arrows point to the TiO_2 shell as determined by EDS.

The infrared spectra of composite catalysts calcined at 400 °C along with the $NiFe_2O_4$ are shown in Fig 4. In the spectrum of calcined pure TiO_2 (T-100-400), very broad Ti-O-Ti framework stretching modes were observed in the range from 1000 to 400 cm^{-1} [43-46]. These vibrations were partially overlapped by the 590 cm^{-1} band of Fe-O stretching vibrations of $NiFe_2O_4$ in the composite catalysts [47, 48]. The intensity of the 590 cm^{-1} peak increased proportionally to $NiFe_2O_4$ content. Also the width of the Fe-O band, which was close for all composite catalysts, was noticeable broader compared to that of $NiFe_2O_4$. This broadening suggests a very close contact between $NiFe_2O_4$ and TiO_2 and confirms the formation of the core-shell structure in agreement with the TEM data (Fig 3).

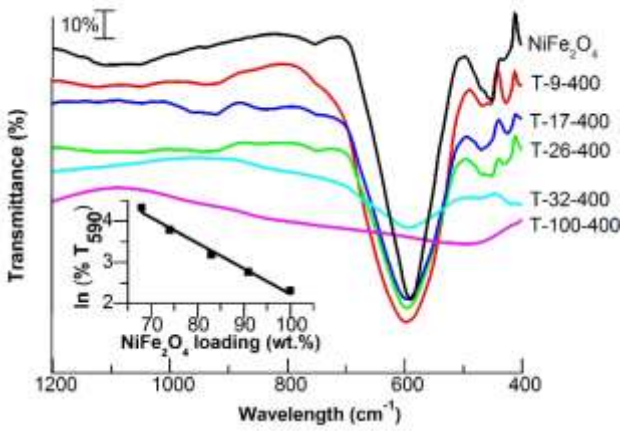

Fig 4. FT-IR spectra of nickel ferrite nanoparticles, as-synthesised TiO_2 (sample T-100-400) and composite catalysts calcined at 400 ºC containing 8.9 wt. % (sample T-9-400), 16.7 wt. % (sample T-17-400), 26.0 wt. % (sample T-26-400) and 32.0 wt. % TiO_2 (sample T-32-400). The spectra are shifted upwards for clarity.

The magnetisation curves of composite catalysts are shown in Fig 5. All the studied composite catalysts showed the same coercivity of 0.2 kG. Because coercivity significantly depends on magnetic particle dimensions, the same coercivity for various catalysts shows that $NiFe_2O_4$ particle dimensions were not affected by the introduction of TiO_2 shell, which is in agreement with TGA (Fig 2) and TEM (Fig 3) data. On increasing titania content, the saturation magnetization linearly decreases because of the decreasing amount of the magnetic $NiFe_2O_4$. The proportionality shows that the saturation magnetization is determined only by the nickel ferrite loading, which means that there is no additional loss of magnetism observed due to the formation of titania shell (see Insert in Fig 5). The specific absorption rate (SAR) of composite catalysts is directly proportional to the area of hysteresis loop between the magnetisation curves, decreasing from 1.08 to 0.88 W g^{-1} as TiO_2 increased from 8.9 to 32 wt. % (Table 2). These data demonstrate that the RF heating properties of the composite catalysts can be precisely controlled during the preparation stage.

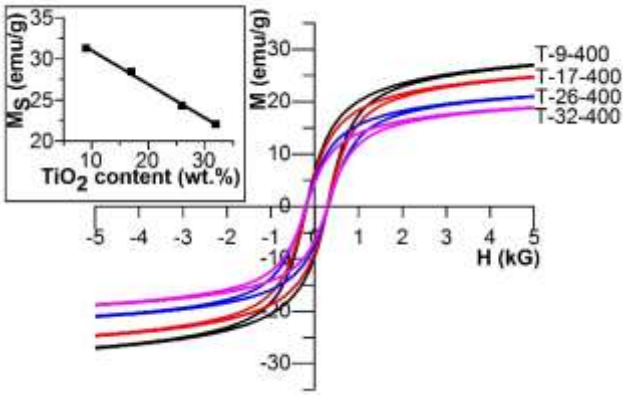

Fig 5. Magnetization curves of composite catalysts with different TiO_2 loading calcined at 400 ºC.

3.3 Effect of calcination temperature

The calcination temperature has a major influence on the phase composition of the resulting composite catalysts. The calcination step is necessary to remove the remaining structure directing agent (CTAB) from the porous network and the temperature should be sufficiently high for its full oxidation (Fig 2). Moreover, the temperature should provide transition of titania into catalytically active anatase phase, but not high enough for the sintering or conversion into less active rutile phase [49, 50]. The effect of calcination temperature on specific surface area and specific absorption rate under RF heating was studied with the composite catalyst having a titania loading of 26 wt. %. According to TGA analysis, the temperature around 500 ºC was high enough to remove the surfactants. The literature shows that the formation of anatase takes place around 400 ºC followed by its transition to rutile above 500 ºC [51]. Hence, the catalysts were calcined at temperatures of 350, 400, 450 and 500 ºC to study phase composition and check for possible core-shell interaction. XRD spectra of the composite catalysts calcined at various temperatures are shown in Fig 6. The formation of anatase phase started at 450 ºC. The XRD peaks at 25.4 and 48.2 °2θ could be attributed to the (101), (200) crystal planes of anatase respectively (JCPDS card 78-2486). The crystallinity of TiO_2 increased with an increase in the calcination temperature from 450 to 500 ºC as it can be seen from the peak intensity of the characteristic anatase peaks at 25.4 °2θ. The peaks at 30.7, 36.0, 37.6, 43.8, 54.8, 58.1 and 64.4 °2θ were assigned to $NiFe_2O_4$ (JCPDS card 74-2081). The small peaks at 31.4 and 41.3 °2θ were assigned to the (220) and (113) crystal planes of α-Fe_2O_3 (JCPDS card 33-0664), which could be typically found as an impurity in the nickel ferrite [41]. The size of $NiFe_2O_4$ crystallites in the catalysts was estimated using a Scherrer equation for the highest intensity (311) peak of $NiFe_2O_4$ to be 52-57 nm for the initial and calcined catalysts, which agreed with the TEM data. Hence, the

calcination temperature of 450 – 500 ºC was beneficial considering anatase formation, while neither core-shell interaction nor rutile formation occurred.

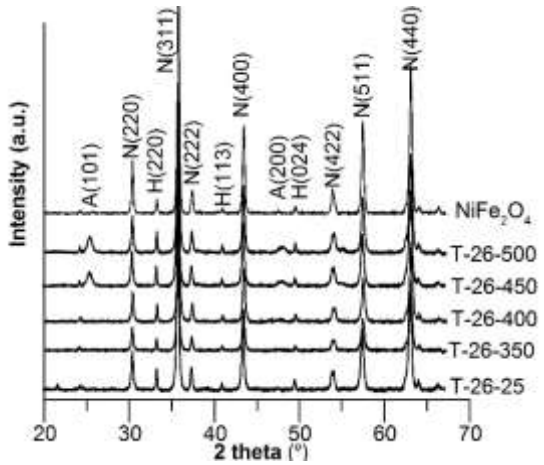

Fig 6. XRD patterns of nickel ferrite nanoparticles ($NiFe_2O_4$) and the composite catalysts containing 26 wt. % titania uncalcined (T-26-25), calcined at 350 ºC (T-26-350), 400 ºC (T-26-400), 450 ºC (T-26-450), 500 ºC (T-26-500). The peaks are assigned to (N) $NiFe_2O_4$, (A) anatase titania, (H) hematite Fe_2O_3. The spectra are shifted upwards for clarity.

The specific surface area and SAR values of calcined catalysts are listed in Table 2. Comparing the catalysts calcined at various temperatures with the initial (T-26-25) catalyst, the specific surface area and SAR decreased by 30 % after calcination at 350 ºC. The decrease in the surface area was likely caused by condensation and densification of the amorphous titania network resulting in the increase in TiO_2 particle sizes, which was observed for many porous materials [52-54].

The decrease in SAR values on calcination requires some discussion of heating mechanisms. There are four mechanisms of heating in RF field: (i) Néel relaxation, (ii) Brownian rotation, (iii) hysteresis loss and (iv) eddy currents (significant only on the centimetre scale materials). The mechanisms were discussed in details in our review[34] as well as in the review of Deatsch and Evans [55] Briefly, Brownian rotation is caused by rotation of magnetic particles in the field with the heat generated via shear stress of the surrounding fluid, Néel relaxation involves rotation of the magnetic moment without the particle movement, and hysteresis loss results in shifting of magnetic domains in multidomain materials [55, 56]. Hence, for the studied particles about of 50 nm in diameter, all three mechanisms are expected because the superparamagnetic and single domain diameters for $NiFe_2O_4$ are 28 and 100 nm, respectively [57, 58].

For the series of core-shell catalysts containing 26 wt. % of titania, an increase in calcination temperature from 350 to 500 ºC resulted in a minor increase in SAR values. A much higher value of the uncalcined materials T-26-25 might be caused by a significantly different surface properties

which provide a stronger interaction with the solvent (water) resulting in a higher Brownian heat generation. Comparing the materials with different titania loading calcined at 500 ºC, the SAR values decreased steadily with increasing titania content (Table 2). This phenomenon was obviously associated with the decrease in $NiFe_2O_4$ content as the SAR value for non-magnetic titania is 0.

Table 2. Specific BET surface area of pristine ($S_{BET,\ initial}$) and spent ($S_{BET,\ spent}$) composite catalysts and specific absorption rate (SAR) for the pristine catalysts.

Sample	$S_{BET,\ initial}$ ($m^2\ g^{-1}$)	$S_{BET,\ spent}$ ($m^2\ g^{-1}$)	SAR ($W\ g^{-1}$)
T-26-25	44.9	n.d.	1.00
T-26-350	31.8	n.d.	0.73
T-26-400	30.7	n.d.	0.76
T-26-450	32.4	n.d.	0.86
T-26-500	35.1	26.7	0.87
T-9-500	21.9	15.6	1.08
T-17-500	25.0	20.0	1.05
T-32-500	51.9	40.8	0.88
P-25	50.5	n.d.	0.00

n.d – not determined

3.4 Catalytic activity and stability

The catalytic activity of composite catalysts was studied in a stirred tank reactor (Fig 7) with the reaction rates normalised for the weight of TiO_2 in the composite catalysts. The reaction rate increased with the calcination temperature from 350 to 500 ºC in agreement with the formation of catalytically active anatase phase observed by XRD study (Fig 6). Remarkably, the samples calcined at 450 and 500 ºC demonstrated similar reaction rates, which were 2.5 times higher than that over the catalyst calcined at 350 ºC. An increase in the specific surface area for the T-26-500 compared to T-26-450 sample might have also contributed to a slightly increased reaction rate (Table 2). Importantly, the reaction rate over composite catalyst T-26-500 normalised per titania weight reached the value of that observed over the reference P25 catalyst. This clearly demonstrates that magnetic functionality can be introduced into catalysts without affecting their catalytic performance. It should be noted that in spite of a rather high reaction temperature of 150 ºC and a single combination of acid and amine, the approach is suitable for a wide range of other substrates.[63] We

anticipate that for thermoliable substrates (such as chiral compounds) much lower reaction rates are expected as the temperature should be reduced far below 150 ºC. Yet, the overall production rate can be kept similar by incresing the catalyst loading in the reactor. The current method allows fast and reproducible preparation of larger amounts of composite catalysts in a very reproducible way.

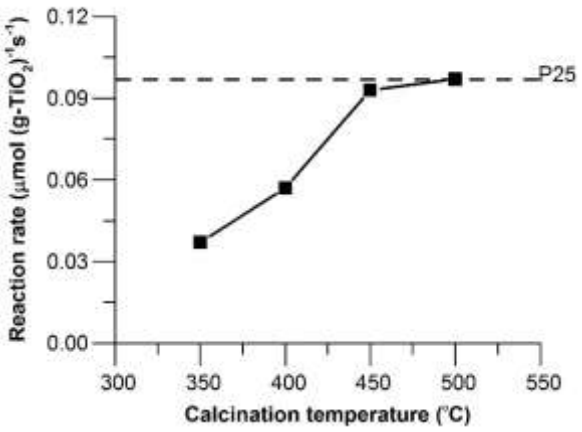

Fig 7. Reaction rate of amide synthesis over composite catalysts containing 26 wt. % titania as a function of calcination temperature in a batch reactor. Reaction conditions: temperature: 150 ºC, pressure: 6 bar, concentration of aniline: 0.05 M in p-xylene, concentration of 4-phenylbutyric acid: 0.05 M in p-xylene, catalyst weight: 680 mg, The dashed line designates the reaction rate over the commercial P-25 catalyst.

To transfer the process to a continuous flow reactor, the benefits of the RF heating were verified first. The performance of RF-heated and conventionally-heated fixed bed reactors filled with the same T-32-500 catalyst was compared (Fig 8) showing an increase in the reaction rate by 60 % in the RF-heated reactor. This difference increased further in the course of the reaction caused likely by different temperature distribution in the studied reactors. In the conventionally-heated flow reactor, heat was transferred from the outer surface via the reactor wall to the composite catalyst, which resulted in a radial temperature gradient in the reactor. On the contrary, the heat was released inside the composite catalyst particles in the RF-heated reactor. As the heated liquid flows downstream, this created an axial temperature gradient, which was reduced by placing inert particles between the catalyst zones[59, 60]. Therefore, one might conclude that the reaction rate could be improved without accelerating deactivation kinetics under RF heating.

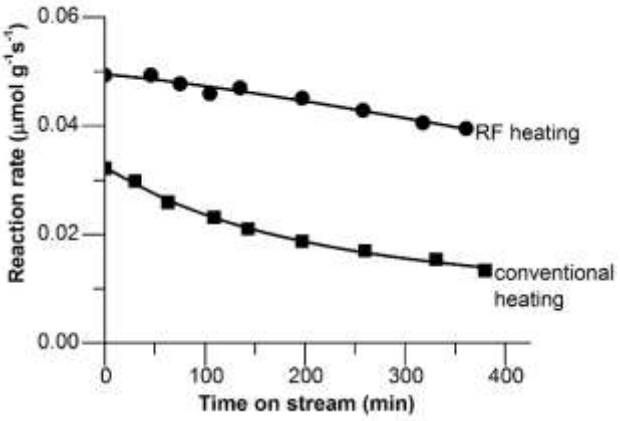

Fig 8. Reaction rate of amide synthesis over the T-32-500 catalyst in conventionally and RF-heated flow reactors as a function of time on stream. Reaction conditions: aniline, 0.1 M in p-xylene at 20 μL min^{-1} and, 4-phenylbutyric acid, 0.1 M in p-xylene at 20 μL min^{-1} introduced in a fixed bed reactor at 150 ºC, pressure 7 bar (g), catalyst weight, 320 mg.

To explore the effect of titania content, the catalytic activity of core-shell composite catalysts with different TiO_2 loadings was studied in the RF-heated flow reactor. Because the SAR values of these catalysts were different, the intensity of magnetic field (electric current in the RF coil) was adjusted in these experiments to keep the same temperature of the reaction mixture as listed in Table 3. It can be seen that the RF power needed to maintain the reaction temperature increased from 101 to 142 W as the titania loading increased from 9 to 32 wt. %. The initial reaction rate over the composites catalyst increased at a higher titania content which was expected because of the larger number of the available active sites. However, the initial reaction rate normalized by the weight of TiO_2 showed that the T-9-500 catalyst had a much lower value while those over the other three samples were close to each other (Table 3). These data indicate that in case of a very thin catalyst shell there exists an interaction between the $NiFe_2O_4$ core and titania shell, which is detrimental for catalytic activity. A possible cause is the electronic interaction between TiO_2 and ferrite referred to as photodissolution phenomenon, which was extensively reported in literature [61-64]. When the thickness of titania shell increases, this detrimental effect becomes less pronounced as the relative contribution from the area near the core-shell interface decreases as compared to the total available surface area.

Table 3. The reaction rates over composite catalysts in the RF-heated flow reactor. Aniline, 0.1 M in p-xylene at 20 μL min^{-1} and, 4-phenylbutyric acid, 0.1 M in p-xylene at 20 μL min^{-1} introduced in a fixed bed reactor at 150 ºC, pressure 7 bar (g), catalyst weight, 320 mg.

Sample	Power input (W)	Initial reaction rate		Initial specific reaction rate x10^4 (μmol m^{-2} s^{-1})	Specific reaction rate in spent catalyst x10^4 (μmol $m^{-2}s^{-1}$)
		μmol $g^{-1}s^{-1}$	μmol g-$TiO_2^{-1}s^{-1}$		
T-9-500	101	0.0048	0.05	2.4	1.5
T-17-500	117	0.023	0.14	9.9	7.5
T-26-500	134	0.030	0.12	9.0	8.3
T-32-500	142	0.049	0.15	9.7	10.1

A strong deactivation was observed during the direct amide synthesis as shown in Figs 8 and 9. The deactivation was likely caused by the formation of trace amounts of azobenzene species on the catalyst surface which readily decompose to form coke and block the catalyst surface [32, 65]. The deactivation was observed in both RF-heated and conventionally-heated reactors (Fig 8). A similar effect was reported in the synthesis performed under microwave heating [66]. The effect of titania loading on deactivation kinetics could be clearly seen when the reaction rate was normalized by the initial reaction rate (Fig 9). Such deactivation behaviour was modelled using a first order kinetics considering slow deactivation caused by blockage of catalysts surface which was caused by the occurring chemical reaction [54, 67]. The corresponding deactivation rate *a* (reaction rate *r* normalised by the initial rate r_0) is presented in Eq. 1

$$a = r / r_0 = \exp(-k_{deactiv}\, t), \qquad (1)$$

where $k_{deactiv}$ is the deactivation constant and *t* is time on stream.

The values of the deactivation constant were inversely proportional to titania loading as shown in Fig 9b. The deactivation rate constant for the catalyst containing 9 wt. % titania was almost 3 times as high as for the catalyst containing 32 wt. % titania. However, this result is not surprising considering that a blockage of an active site for the catalyst containing a small number of sites provides a much higher *relative* deactivation rate compared to the catalyst with a larger number of sites. In fact, the product of the deactivation constant and titania loading (number of active sites) was almost constant for the studied catalysts suggesting the same deactivation mechanism.

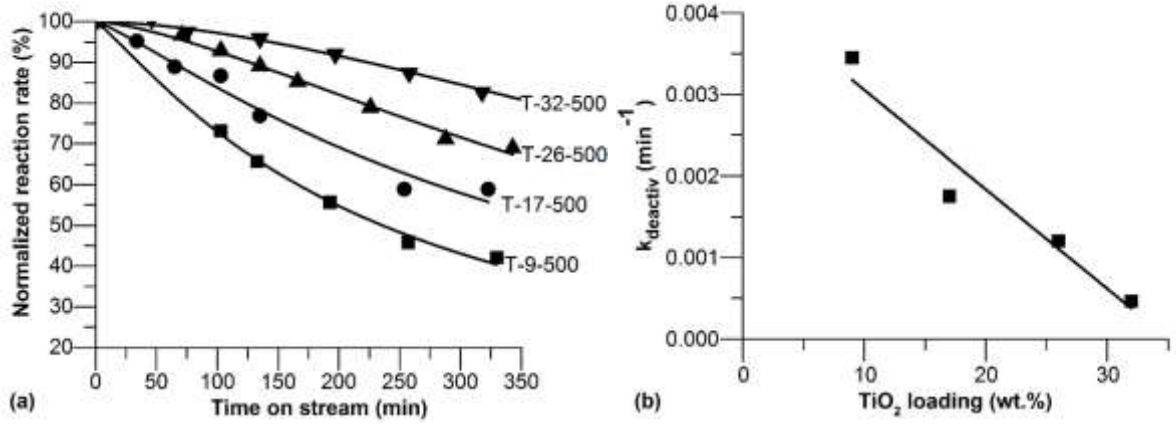

Fig 9. (a) Normalized reaction rate as a function of time on stream and (b) deactivation rate constant as a function of titania loading in the RF-heated flow reactor. . Reaction conditions: aniline, 0.1 M in p-xylene at 20 μL min^{-1} and, 4-phenylbutyric acid, 0.1 M in p-xylene at 20 μL min^{-1} introduced in a fixed bed reactor at 150 ºC, pressure 7 bar (g), catalyst weight, 320 mg.

After 20 h on stream, the surface area of the spent catalysts decreased by 20-25 % (Table 2). However the specific reaction rate (normalised per unit of surface area) remained virtually the same (9.7×10^{-4} vs 10.1×10^{-4} μmol $m^{-2}s^{-1}$) in the spent ST-32-500 catalyst having the highest titania loading while the reaction rate slightly reduced in the catalysts with lower titania loadings (Table 3). Hence, it can be concluded that both reduced surface area and site blockage are responsible for deactivation. These processes may occur separately or they can be caused by the same reason such as surface coking.

In order to study the deactivation mechanism, the temperature programmed oxidation (TPO) study of spent catalysts was performed. Fig 10 shows CO_2 profiles obtained in the TPO experiments over the spent catalysts. It should be mentioned that these concentration profiles were normalized per titania weight in the catalysts. The CO_2 peaks at 260, 350 and 465 ºC indicate three types of carbon species formed during the reaction. The amount of carbon species was the highest in the spent catalyst with the lowest titania loading and it gradually decreased as the amount of titania increased. The ST-9-500 catalyst had also the highest amount of strongly adsorbed carbon species which require a temperature in excess of 475 ºC for their complete oxidation. The coke was likely formed on hot spots and required higher temperatures to be removed than the coke obtained on the catalysts with higher amounts of titania.

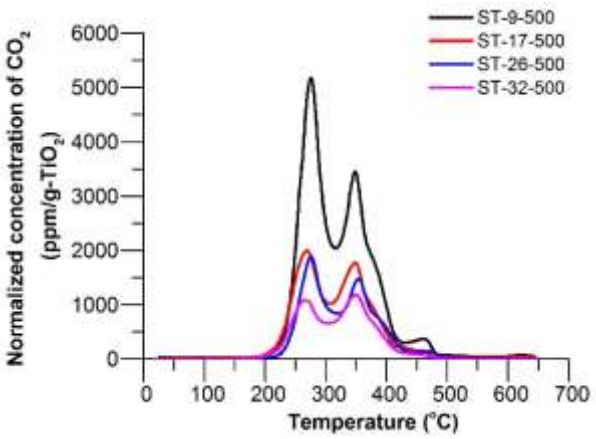

Fig 10. Normalized CO_2 profiles over spent catalysts in TPO experiments with a heating rate of 5 ^oC min^{-1} in the flow of 20 vol. % O_2/N_2.

The catalyst regeneration from coke is typically performed by calcination in air. The carbon from the spent T-32-500 catalyst can be fully removed by the calcination at 400 ^oC for 1 h as demonstrated by the TPO experiment (Fig 11). However, even despite of very low calcination temperature, this procedure reduced the surface area in the regenerated catalyst by 12 %, to 30.2 m^2 g^{-1}, likely because of sintering of the porous titania shell. As a result, the reaction rate in the amide synthesis over the recovered catalyst in the second catalytic run was not fully recovered after regeneration (Fig 12).

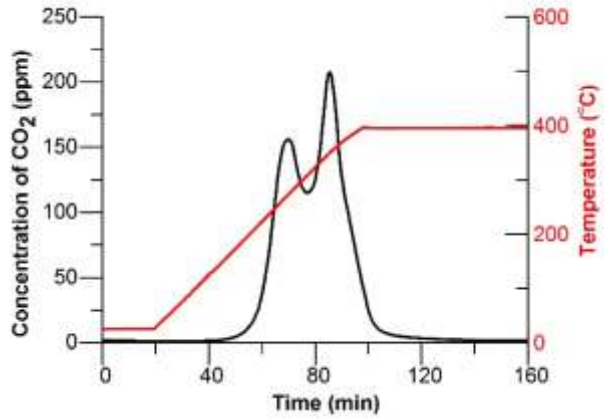

Fig 11. CO_2 profile over the spent ST-32-500 in a TPO experiment with a heating rate of 5 °C min^{-1} in the flow of 20 vol. % O_2/N_2.

To minimise sintering, the catalyst regeneration temperature has to be decreased. Obviously, calcination in air cannot be performed at the temperature much lower than 400 °C (Fig 11), hence other decoking agents should be employed. Querini et al. [68] successfully used a hydrogen peroxide

solution for catalyst regeneration as a low-temperature oxidation agent. Following this approach, the surface area of the regenerated composite catalyst was determined to be 48.5 m^2 g^{-1}, which was marginally lower than that in the fresh catalyst of 51.9 m^2 g^{-1}. The results of the catalyst testing of this mildly-regenerated catalysts (CT-32-500) show that the catalytic activity was fully restored (Fig 12). Also the second catalytic run followed the same deactivation kinetics as the first run indicating that the catalyst was returned to the initial state after the treatment with the hydrogen peroxide solution. It can be concluded that the dominant deactivation mechanism is associated with the formation of coke.

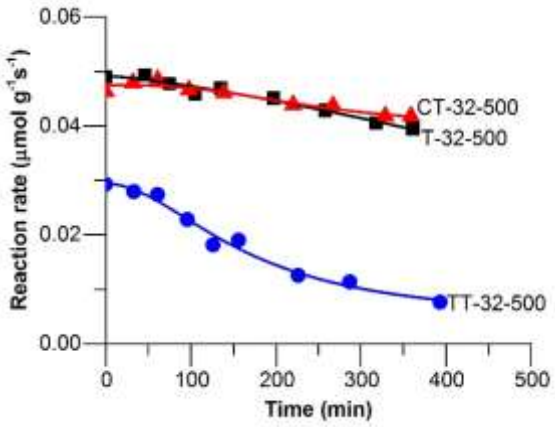

Fig 12. Reaction rate in the RF-heated flow reactor as a function of time over different composite catalysts: as synthesized T-32-500 catalyst, the same spent catalyst after calcination in air at 400 ºC for 1 h (TT-32-500), and after chemical regeneration with hydrogen peroxide (CT-32-500) at 90 ºC for 22 h. Reaction conditions: aniline, 0.1 M in p-xylene at 20 μL min^{-1} and, 4-phenylbutyric acid, 0.1 M in p-xylene at 20 μL min^{-1} introduced in a fixed bed reactor at 150 ºC, pressure 7 bar (g), catalyst weight, 320 mg.

4. Conclusions

Core-shell TiO_2@$NiFe_2O_4$ composite catalysts have been prepared by sol-gel method. By adjusting the amount of titania precursor in the initial synthesis sol, it has been possible to precisely control titania loading as well as specific absorption rate of the catalysts. Thermogravimetric and X-ray studies showed that no chemical reaction occurs between the magnetic core and the catalytic titania shell below 500 ºC. The optimisation of the catalyst calcination temperature demonstrated that the transition of titania into catalytically active anatase phase started at 450 ºC, resulting in the highest catalytic activity of the catalyst calcined at 500 ºC and no sintering of the titania shell was observed.

The catalytic activity was compared in the direct amide synthesis from aniline and 4-phenylbutyric acid in a fixed-bed continuous flow reactor under conventional heating and RF heating. The initial reaction rate was by 60 % higher under RF heating. The deactivation rate was higher in the conventionally-heated reactor due to the presence of a radial temperature gradient. This allows significant process intensification in RF-heated reactors loaded with composite catalysts.

The catalyst deactivation behaviour was studied for a range of catalysts calcined at 500 ^{o}C and having various titania loading in the range of 9–32 wt. %. The reaction rate normalised by titania weight was constant over the catalysts with titania loadings above 17 wt. %. However, the catalyst with a 9 wt. % titania loading showed significantly lower reaction rate because of a negative influence of the magnetic core onto the catalytic shell as a result of their electronic interaction near the interface. The catalyst deactivation rate was described by a first order kinetics demonstrating deactivation rate constant was inversely proportional to the thickness of titania shell.

The analysis of deactivated catalysts showed that coking was the main deactivation mechanism. The coke was fully removed by calcination in air at 400 ^{o}C leading to sintering of titania and a non-reversible catalyst deactivation. No sintering of titania was observed after the regeneration with a 30 wt. % H_2O_2 solution at 90 ^{o}C. This regeneration procedure provided full recovery of the catalytic properties. It can be concluded that a combination of a core-shell composite catalyst with a continuous flow mode provides a promising way for direct amide synthesis with easy catalyst regeneration and magnetic separation.

Acknowledgements

The financial support provided by the European Research Council (ERC) project 279867 and the Russian Science Foundation project 15-13-20015 is gratefully acknowledged.

References

1. J. S. Carey, D. Laffan, C. Thomson and M. T. Williams, *Organic & Biomolecular Chemistry*, 2006, **4**, 2337-2347.
2. J.-F. Soulé, H. Miyamura and S. Kobayashi, *Journal of the American Chemical Society*, 2011, **133**, 18550-18553.
3. V. R. Pattabiraman and J. W. Bode, *Nature*, 2011, **480**, 471-479.
4. D. J. Constable, P. J. Dunn, J. D. Hayler, G. R. Humphrey, J. L. Leazer Jr, R. J. Linderman, K. Lorenz, J. Manley, B. A. Pearlman and A. Wells, *Green Chemistry*, 2007, **9**, 411-420.
5. E. Valeur and M. Bradley, *Chemical Society Reviews*, 2009, **38**, 606-631.
6. C. Chen and Q. Wu, *RSC Advances*, 2016.
7. R. M. Lanigan, P. Starkov and T. D. Sheppard, *The Journal of organic chemistry*, 2013, **78**, 4512-4523.
8. H. Charville, D. A. Jackson, G. Hodges, A. Whiting and M. R. Wilson, *European Journal of Organic Chemistry*, 2011, **2011**, 5981-5990.
9. R. S. Varma and K. P. Naicker, *Tetrahedron letters*, 1999, **40**, 6177-6180.

10. S. H. Siddiki, A. S. Touchy, M. Tamura and K.-i. Shimizu, *RSC Advances*, 2014, **4**, 35803-35807.
11. F. Arena, C. Deiana, A. F. Lombardo, P. Ivanchenko, Y. Sakhno, G. Trunfio and G. Martra, *Catalysis Science & Technology*, 2015, **5**, 1911-1918.
12. P. S. Chaudhari, S. D. Salim, R. V. Sawant and K. G. Akamanchi, *Green Chemistry*, 2010, **12**, 1707-1710.
13. J. W. Comerford, J. H. Clark, D. J. Macquarrie and S. W. Breeden, *Chemical Communications*, 2009, 2562-2564.
14. K. Arnold, A. S. Batsanov, B. Davies and A. Whiting, *Green Chemistry*, 2008, **10**, 124-134.
15. M. Hosseini-Sarvari, E. Sodagar and M. M. Doroodmand, *The Journal of organic chemistry*, 2011, **76**, 2853-2859.
16. S. Nagarajan, P. Ran, P. Shanmugavelan, M. Sathishkumar, A. Ponnuswamy and K. S. Nahm, *New Journal of Chemistry*, 2012, **36**, 1312-1319.
17. C. Deiana, Y. Sakhno, M. Fabbiani, M. Pazzi, M. Vincenti and G. Martra, *ChemCatChem*, 2013, **5**, 2832-2834.
18. E. C. Gaudino, D. Carnaroglio, M. G. Nunes, L. Schmidt, E. Flores, C. Deiana, Y. Sakhno, G. Martra and G. Cravotto, *Catalysis Science & Technology*, 2014, **4**, 1395-1399.
19. K. F. Jensen, *Chemical Engineering Science*, 2001, **56**, 293-303.
20. S. V. Ley, D. E. Fitzpatrick, R. Ingham and R. M. Myers, *Angewandte Chemie International Edition*, 2015, **54**, 3449-3464.
21. V. Hessel, D. Kralisch, N. Kockmann, T. Noel and Q. Wang, *ChemSusChem*, 2013, **6**, 746-789.
22. N. Cherkasov, A. O. Ibhadon and E. V. Rebrov, *Catalysis Today*, 2016, **273**, 205-212.
23. D. M. Roberge, L. Ducry, N. Bieler, P. Cretton and B. Zimmermann, *Chemical engineering & technology*, 2005, **28**, 318-323.
24. N. Cherkasov, A. O. Ibhadon and E. V. Rebrov, *Applied Catalysis A: General*, 2016, **515**, 108-115.
25. S. Mascia, P. L. Heider, H. Zhang, R. Lakerveld, B. Benyahia, P. I. Barton, R. D. Braatz, C. L. Cooney, J. Evans and T. F. Jamison, *Angewandte Chemie International Edition*, 2013, **52**, 12359-12363.
26. T. Gustafsson, F. Pontén and P. H. Seeberger, *Chemical Communications*, 2008, 1100-1102.
27. X. Liu and K. F. Jensen, *Green Chemistry*, 2013, **15**, 1538-1541.
28. J. D. Moseley and C. O. Kappe, *Green Chemistry*, 2011, **13**, 794-806.
29. S. Ceylan, C. Friese, C. Lammel, K. Mazac and A. Kirschning, *Angewandte Chemie International Edition*, 2008, **47**, 8950-8953.
30. S. R. Chaudhuri, J. Hartwig, L. Kupracz, T. Kodanek, J. Wegner and A. Kirschning, *Advanced Synthesis & Catalysis*, 2014, **356**, 3530-3538.
31. J. Hartwig, S. Ceylan, L. Kupracz, L. Coutable and A. Kirschning, *Angewandte Chemie International Edition*, 2013, **52**, 9813-9817.
32. T. K. Houlding, P. Gao, V. Degirmenci, K. Tchabanenko and E. V. Rebrov, *Materials Science and Engineering: B*, 2015, **193**, 175-180.
33. W. Sun, W. Yang, Z. Xu, Q. Li and J. K. Shang, *ACS applied materials & interfaces*, 2016, **8**, 2035-2047.
34. T. K. Houlding and E. V. Rebrov, *Green Processing and Synthesis*, 2012, **1**, 19-31.
35. T. Feczkó, A. Muskotál, L. Gál, J. Szépvölgyi, A. Sebestyén and F. Vonderviszt, *Journal of Nanoparticle Research*, 2008, **10**, 227-232.
36. G. Chen, S. Desinan, R. Nechache, R. Rosei, F. Rosei and D. Ma, *Chemical Communications*, 2011, **47**, 6308-6310.
37. Z. Xu, Y. Hou and S. Sun, *Journal of the American Chemical Society*, 2007, **129**, 8698-8699.
38. J. Ge, Q. Zhang, T. Zhang and Y. Yin, *Angewandte Chemie*, 2008, **120**, 9056-9060.
39. P. Gao, X. Hua, V. Degirmenci, D. Rooney, M. Khraisheh, R. Pollard, R. M. Bowman and E. V. Rebrov, *Journal of Magnetism and Magnetic Materials*, 2013, **348**, 44-50.
40. K. Maaz, S. Karim, A. Mumtaz, S. Hasanain, J. Liu and J. Duan, *Journal of Magnetism and Magnetic Materials*, 2009, **321**, 1838-1842.
41. A. Paladino, *Journal of the American Ceramic Society*, 1959, **42**, 168-175.
42. S. Bagheri, F. Chekin and S. B. A. Hamid, *Russian Journal of Electrochemistry*, 2014, **50**, 947-952.
43. J. Ropero-Vega, A. Aldana-Pérez, R. Gómez and M. Niño-Gómez, *Applied Catalysis A: General*, 2010, **379**, 24-29.
44. J. Lei, Y. Chen, F. Shen, L. Wang, Y. Liu and J. Zhang, *Journal of Alloys and Compounds*, 2015.
45. K. Priyanka, P. Sheena, N. A. Sabu, T. George, K. Balakrishna and T. Varghese, *Indian Journal of Physics*, 2014, **88**, 657-663.
46. G. Khade, M. Suwarnkar, N. Gavade and K. Garadkar, *Journal of Materials Science: Materials in Electronics*, **26**, 3309-3315.

47. A. B. Rajput, S. J. Rahaman, G. Sarkhel, M. K. Patra, S. R. Vadera and N. N. Ghosh, *Polymer-Plastics Technology and Engineering*, 2013, **52**, 1097-1105.
48. S. Maensiri, C. Masingboon, B. Boonchom and S. Seraphin, *Scripta Materialia*, 2007, **56**, 797-800.
49. X. Liang and R. L. Patel, *Ceramics International*, 2014, **40**, 3097-3103.
50. D. J. Kim, S. H. Hahn, S. H. Oh and E. J. Kim, *Materials Letters*, 2002, **57**, 355-360.
51. D. A. Hanaor and C. C. Sorrell, *Journal of Materials science*, 2011, **46**, 855-874.
52. H. Chen, K. Dai, T. Peng, H. Yang and D. Zhao, *Materials chemistry and physics*, 2006, **96**, 176-181.
53. S.-Y. Chen, L.-Y. Jang and S. Cheng, *The Journal of Physical Chemistry B*, 2006, **110**, 11761-11771.
54. C. H. Bartholomew, *Applied Catalysis A: General*, 2001, **212**, 17-60.
55. A. E. Deatsch and B. A. Evans, *Journal of Magnetism and Magnetic Materials*, 2014, **354**, 163-172.
56. M. Beković and A. Hamler, *Magnetics, IEEE Transactions on*, 2010, **46**, 552-555.
57. I. Sharifi, H. Shokrollahi and S. Amiri, *Journal of Magnetism and Magnetic Materials*, 2012, **324**, 903-915.
58. M. Kooti and A. N. Sedeh, *Journal of Materials Science & Technology*, 2013, **29**, 34-38.
59. S. Chatterjee, V. Degirmenci, F. Aiouache and E. V. Rebrov, *Chemical Engineering Journal*, 2014, **243**, 225-233.
60. S. Chatterjee, V. Degirmenci and E. V. Rebrov, *Chemical Engineering Journal*, 2015, **281**, 884-891.
61. D. Beydoun, R. Amal, G. Low and S. McEvoy, *Journal of Molecular Catalysis A: Chemical*, 2002, **180**, 193-200.
62. Q. Yuan, N. Li, W. Geng, Y. Chi and X. Li, *Materials Research Bulletin*, 2012, **47**, 2396-2402.
63. Y. Chi, Q. Yuan, Y. Li, L. Zhao, N. Li, X. Li and W. Yan, *Journal of hazardous materials*, 2013, **262**, 404-411.
64. A. Costa, B. Ballarin, A. Spegni, F. Casoli and D. Gardini, *Journal of colloid and interface science*, 2012, **388**, 31-39.
65. T. K. Houlding, K. Tchabanenko, M. T. Rahman and E. V. Rebrov, *Organic & biomolecular chemistry*, 2013, **11**, 4171-4177.
66. E. Gelens, L. Smeets, L. A. Sliedregt, B. J. van Steen, C. G. Kruse, R. Leurs and R. V. Orru, *Tetrahedron letters*, 2005, **46**, 3751-3754.
67. P. Forzatti and L. Lietti, *Catalysis today*, 1999, **52**, 165-181.
68. C. A. Querini, *Catalysis today*, 2000, **62**, 135-143.